Advances in Materials Research, *Vol. 11, No. 4 (2022) 351-374*
https://doi.org/10.12989/amr.2022.11.4.351

Determining a novel softening function for modeling the fracture of concrete

Hossein Karimpour[a] and Moosa Mazloom*

Department of Civil Engineering, Shahid Rajaee Teacher Training University, Lavizan, Tehran, Iran

(*Received August 11, 2021, Revised April 18, 2022, Accepted April 22, 2022*)

Abstract. Softening function is the primary input for modeling the fracture of concrete when the cohesive crack approach is used. In this paper, based on the laboratory data on notched beams, an inverse algorithm is proposed that can accurately find the softening curve of the concrete. This algorithm uses non-linear finite element analysis and the damage-plasticity model. It is based on the kinematics of the beam at the late stages of loading. The softening curve, obtained from the corresponding algorithm, has been compared to other softening curves in the literature. It was observed that in determining the behavior of concrete, the usage of the presented curve made accurate results in predicting the peak loads and the load-deflection curves of the beams with different concrete mixtures. In fact, the proposed algorithm leads to softening curves that can be used for modeling the tensile cracking of concrete precisely. Moreover, the advantage of this algorithm is the low number of iterations for converging to an appropriate answer.

Keywords: cohesive crack model; concrete; fracture process zone; inverse analysis; softening curve

1. Introduction

1.1 Research background

Concrete is a quasi-brittle material that has been widely used in structures for the last decades. Because of the quasi-brittle nature of this material, the existence of microcracks is inevitable, leading to stable growth of the cracking zone and the failure of the concrete element before the maximum load is reached. Due to the limitation of strength criteria, engineers should consider the fracture criteria to have a better prediction of concrete elements' response under monotonic and cyclic loadings. The application of fracture mechanics is essential mainly for structures with high safety concerns, such as concrete dams and nuclear reactor vessels or containments (Bazant 2003, Karamloo and Mazloom 2018).

The components of concrete, a heterogeneous material, are aggregates and cement paste bonded to each other at the interfacial transition zone (ITZ). Due to the limited bonding strength as well as the micro-cracks and flaws that occur during the hardening of the matrix, concrete has a low tensile strength (Mehta and Monteiro 2017).

Under an external load, a tension zone forms adjacent to the crack tip; therefore, complex

*Corresponding author, Professor, E-mail: Mazloom@sru.ac.ir
[a]Ph.D., E-mail: karimpour.h@sru.ac.ir, karimpour.h@gmail.com

http://www.techno-press.org/?journal=amr&subpage=5 ISSN: 2234-0912 (Print), 2234-179X (Online)

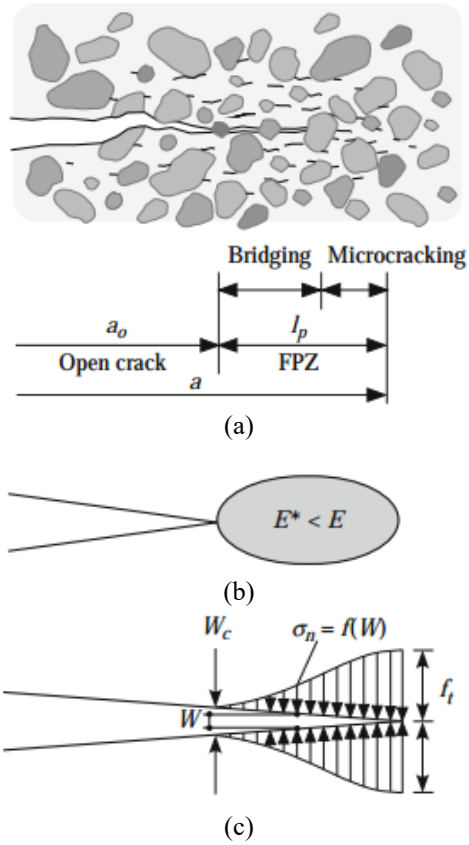

Fig. 1 (a) FPZ location (b) Reduced elasticity modulus in the vicinity of the crack-tip (c) Cohesive stresses acting on the crack faces (Shi 2009)

micro-failure mechanisms occur in that region (Afzali *et al.* 2019, Salehi and Mazloom 2019a, Mazloom *et al.* 2020, Abna and Mazloom 2022). Fracture processes that cause energy absorption at the crack tip are called "crack inelastic toughening mechanisms." The mechanisms of micro failure are micro cracking, crack deflection, crack branching, crack coalescence, and aggregate debonding from the hydrated cement matrix (Pavlovic 1996). Due to the development of the inelastic zone at the crack tip, linear elastic fracture mechanics, LEFM, cannot be used to analyze concrete failure (Salehi and Mazloom 2019b, Mazloom *et al.* 2021). Fig. 1 schematically shows the formation of the inelastic zone at the crack tip, called the fracture process zone (FPZ). FPZ is ideally composed of two zones: the bridging zone and the microcracking zone (Shi 2009).

The bridging zone as an essential toughening mechanism results from a weak interface between aggregates and the matrix. According to Shi (2009), in the fracture process zone (FPZ), the effective modulus of elasticity (E*) reduces, and its value is lower than the elastic modulus of the undamaged parts of the material (E).

Hillerborg *et al.* (1976) imagined a fictitious instead of physical fracture process zone (FPZ). This assumption is the concept of cohesive zone models, suggested by Dugdale (1960) and Barenblatt (1962). The fictitious crack is exposed to the closure tractions, as shown in Fig. 1(c). The closure stresses are mainly related to bridging grains and the presence of micro-cracks. As

shown in Fig. 1, the stress at the tip of the fictitious crack is the maximum stress, which is equal to the tensile strength of concrete (f_t') (Hillerborg *et al.* 1976). These cohesive stresses correspond to the crack openings, and they reduce along the fictitious crack to zero, where the concrete opening displacement reaches its critical value (W_C). At the faces of the crack where the crack opening is more than the critical value, the traction-free surface and the real crack form (Hillerborg *et al.* 1976).

The relation between the cohesive stress acting across the crack faces and the crack opening, known as softening function, describes the local behavior of the material inside the FPZ when the fracture occurs in the material.

It is worth noting that constitutive relations of continuous materials explain the fundamental behavior of the materials in compression and tension. Moreover, the function of traction separation and fracture energy are the main constitutive parameters for materials in FPZ. The traction separation function stipulates the transitional behavior of material from a continuous state to a discontinuous one. It clarifies how an increase in discontinuity in FPZ affects tension stresses at the crack tip (Shi 2009).

Researchers found the shape of this constitutive relationship by using control displacement uniaxial tensile tests or other creative methods such as inverse methods. The narrow prismatic specimen was used by Reinhardt *et al.* (1986) to find the softening curve of concrete by the deformation-controlled uniaxial tests. The specimens had two saw-cuts. It was found that during the first stages of the tension test, the FPZ was not established at the same time as the initial micro cracks spread. It was established after the load reached its maximum value and the deformation of the specimen localized in the FPZ in this stage (Reinhardt *et al.* 1986).

There are some deficiencies in performing direct tensile tests for obtaining softening curves, such as difficulties in propagating cracks stably and the dependence of the result on the size and shape of the specimen (Reinhardt *et al.* 1986, Van Mier 1986). For these reasons, most of the methods for finding the softening law depend on indirect approaches that are based on the parametric fit of experimental results obtained from bending beams or compact specimens (Wittmann *et al.* 1987, 1988).

Li *et al.* (1987) proposed the J-integral method to obtain the softening curve. Miller *et al.* (1991) got the softening law from crack profiles by laser holography interferometry. Moire interferometry was used by Yon *et al.* (1997). Alam and Loukili (2020) considered the effects of the micro-macro crack in traction on the softening function utilizing digital image correlation and acoustic emission techniques. They showed that the micro-cracks interact with the macro-cracks and disrupt its smooth opening as the crack grows.

Many researchers have used inverse analysis to find the softening function. The wedge splitting test setup was applied experimentally by Østergaard *et al.* (2004). They used an inverse algorithm to extract the softening function. It was based on the non-linear cracked hinge model, which uses the fictitious crack concept for interpreting the results.

In recent years, the fracture behavior of fiber-reinforced cementitious composites at ambient and elevated temperatures has also been considered (Karimpour and Mazloom 2022, Mazloom and Mirzamohammadi 2019, 2021a, 2021b). Reddy and Subramaniam (2017), using the inverse analysis and cracked hinge model, introduced an analytical formulation for macro-synthetic fiber reinforced concrete, in which the multi-linear cohesive stress-crack opening relationship was found from the flexural notched beam response. Bhosale *et al.* (2020) developed a softening function for hybrid fiber reinforced concrete (HFRC). They performed an inverse analysis based on the fictitious crack hinge model to derive the softening law by carefully calibrating model

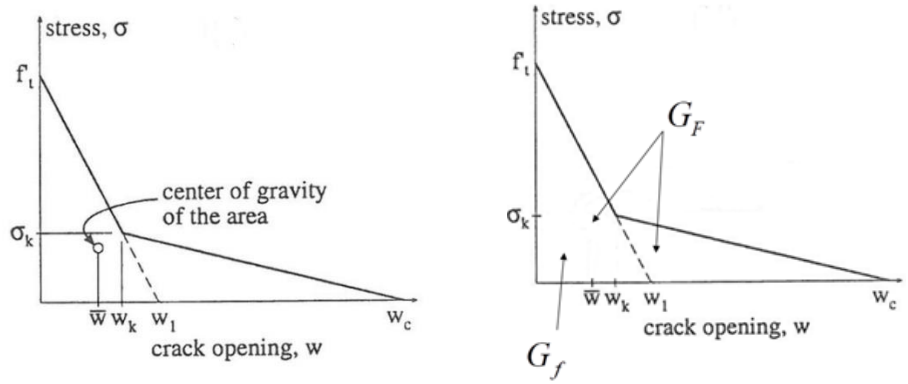

(a) (b)

Fig. 2 Bilinear softening function (Bazant and Planas 2019)

Table 1 Softening models for concrete

Hillerborg et al. (1976)	Linear softening curve (G_F, f_t')
Petersson (1981) Gustafsson and Hillerborg (1985)	Bilinear softening curve (G_F, f_t') Fixed kink point at $(\frac{0.8G_F}{f_t'}, \frac{f_t'}{3})$
Wittmann *et al.* (1988)	Bilinear softening curve (G_F, f_t') Fixed stress kink point $0.25f_t'$
Park *et al.* (2008)	Bilinear softening curve(G_F, G_f, f_t') Assume $w_k = CTOD_C$
Ceb-Fip (1990)	Bilinear softening curve (G_F, f_t', d_{max}) Fixed kink point at $(\frac{G_F}{f_t'}, 0.15f_t')$
Guinea *et al.* (1994)	Bilinear softening curve (G_F, f_t') Suggest two more empirical parameters for determining the kink point
Zdeněk P. Bažant (2001)	Bilinear softening curve(G_F, G_f, f_t') The stress of the kink point $(\psi f_t')$

parameters with the digital image correlation (DIC) measurements.

1.2 Different softening functions

With the efforts of many researchers, the concept of traction separation law has been accepted as the basis of concrete fracture mechanics. It is obligatory for cohesive crack computations to use the softening function as an input.

Among various functions proposed for the softening of the concrete, such as linear and exponential, the bilinear softening functions have been widely used in the literature; consequently, it is decided to use the bilinear ones in this article.

As shown in Fig. 2, the traction separation relation of concrete has two distinct characteristics. The first is a steep slope descending section due to the rapid loss of tensile strength in the initial softening stage. The second item is a long tail that indicates the consistent stress transfer capacity

of aggregates in the FPZ (Shi 2009).

Table 1 summarizes the most widely used softening laws based on fracture parameters. Hillerborg *et al.* (1976) defined the linear softening law. The model characteristics were the tensile strength (f_t') and the total fracture energy (G_F). They used the cohesive crack model along with the finite element method to analyze concrete structures.

Then, Petersson (1981) suggested a bilinear softening curve. The coordinates of its kink point, the point of the intersection of two lines in the bilinear softening curve, were fixed at ($\frac{0.8G_F}{f_t'}, \frac{f_t'}{3}$). A schematic bilinear softening curve is shown in Fig. 2. This bilinear model was adopted by Gustafsson and Hillerborg (1985), too.

For the numerical assessment, Wittmann *et al.* (1988) recommended a bilinear softening curve with a kink point stress equal to $0.25f_t'$. Park *et al.* (2008) suggested that the location of the kink point (w_k) is the critical crack tip opening displacement (CTOCc).

The Ceb-Fip (1990) proposed a bilinear softening function for Ordinary concrete with different strength levels. It could be defined by the tensile strength of the concrete (f_t'), the total fracture energy(G_F), the maximum aggregate size, and a kink point stress of $0.15f_t'$. The value of critical opening (W_c) depends on the maximum aggregate size. The value of (w_1) is given by Eq. (1) in the units of millimeters. k_d depends on the maximum size of the aggregates.

$$w_1 = \frac{G_F - 22W_c(\frac{G_F}{k_d})^{0.95}}{150\left(\frac{G_F}{k_d}\right)^{0.95}} \quad (1)$$

Guinea *et al.* (1994) defined two experimental parameters to demonstrate the shape of the softening curve.

The above-mentioned softening laws have primarily been defined by two fracture parameters (f_t' and G_F). There is no consensus on the precise location of the kink point. This is not abnormal because different concrete mixtures can have different softening curves. Several methods exist in the literature to find the bilinear softening function and capture the main trends of the fracture processes and the size effect. Some methods usually overestimate the strength of normal-sized specimens (Bazant and Planas 2019).

It is imperative to find a method to identify any bilinear softening curve to fit particular experimental data. This paper presents a new method for inferring the essential properties of the softening function from the experiments performed on notched beams and with the aid of the non-linear finite element method. The proposed algorithm is based on a simple model that determines the bilinear softening curve of plain concrete with limited iterations and with the help of a finite element software available to researchers and engineers. However, this method can only be used in plain concrete with a bilinear softening curve. A multi-linear (σ-w) relationship must be considered for fiber-reinforced concrete using the integration method (Gao *et al.* 2021).

Four algorithm input parameters are estimated from the standard tests. These tests are based on the ASTM Standard C469 (2002) for elastic modulus, the ASTM C 469/C 496M (2004) for splitting tensile strength, and the RILEM work-of-fracture recommendation (1985) for fracture energy. In this study, these parameters are obtained from the results presented by the second author previously (Afzali-Naniz and Mazloom 2019).

The resulting softening curve is compared with other bilinear softening curves found in the literature. The results show that the presented method in this paper leads to more accurate results than the others.

2. The analytical formulation for finding the softening function

The softening functions capture the vital facts that describe the fracture behavior of the concrete. The steepest part represents the large-scale debonding or fracture of aggregates, and the shallow part of the diagram demonstrates the frictional pull-out of aggregate in the concrete (Guinea *et al.* 1994).

Fig. 2 shows the typical curve of the bilinear function.

It can be expressed explicitly as a function of softening curve parameters. In this function, (σ_k, w_k) are the coordinates of the kink point and w_c is the critical opening. The expression of softening function in terms of bilinear softening curve parameters is

$$\sigma = f_t' \left(1 - \frac{w}{w_1}\right), \text{for } 0 \le w \le w_k$$
$$\sigma = \sigma_k \left(\frac{w - w_c}{w_k - w_c}\right), \text{for } w_k \le w \le w_c \quad (2)$$
$$\sigma = 0, \text{for } w \ge w_c$$

As shown in Fig. 2, the parameters that must be identified experimentally to characterize the softening function are the tensile strength (f_t'), the total fracture energy (G_F), and the specific fracture energy (G_f). For finding the tensile strength (f_t') due to the lack of a reliable direct tension test, the researchers use the result of a Brazilian splitting test. The Tensile strength is calculated by an equation, which presumes isotropic material properties (ASTM C 469/C 496M 2004). The total fracture (G_F) is measured by the RILEM standard method. It is based on three-point bending tests on notched beams. The measured value of G_F in this approach is obtained by dividing the measured work of fracture W_F by the original uncracked ligament area (RILEM 1985).

$$G_F = \frac{W_F}{b(d - a_0)} \quad (3)$$

Where W_F is corresponding to the area under the load-displacement curve up to the displacement in which load returns to zero; b is the beam width, d is the beam depth, and a_0 is the initial notch depth of the beam. The specific fracture energy (G_f) is determined based on the size effect method (SEM) proposed by Bazant and Pfeiffer (1987). This method is based on the effective elastic crack model described by Shah (1990). The specific fracture energy (G_f) does not

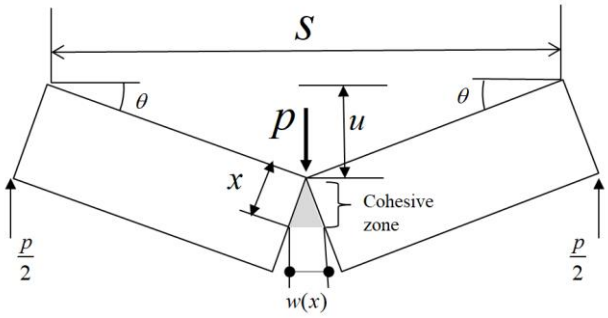

Fig. 3 Rigid body kinematics towards the end of the test

depend on the size and shape of the specimen (ACI 446.3R-97 1997). According to RILEM (1990), the fracture parameters can be determined by three-point bending tests on notched beams with different sizes and similar geometries. The dimensions of the beams depend on the maximum size of aggregate (d_{max}).

Other parameters, which are obligatory for the definition of softening function, are the abscissa of the center of gravity of the softening area ($\overline{w}$), the critical displacement (w_c) and coordinates of the kink point(σ_k, w_k). For finding these parameters, the following steps are suggested.

Consider the free body diagram of the beam, as shown in Fig. 3, in which an approximation of the kinematic of the beam at the late loading stages is depicted. It is presumed that two halves of the beam are rigid and bridged by a cohesive zone (Guinea *et al.* 1994). In the last loading stage, when the crack fully extends at the height of the concrete beam, there are no tensile and compressive stresses in the cross-section except for cohesive stresses applied on both sides of the crack edges (Broujerdian *et al.* 2018). The following equation can calculate the crack opening

$$\omega = 2\theta x \tag{4}$$

In Eq. (4), x is shown in Fig. 3, and θ is the rotation of each half of the specimen. The angle θ is assumed to be small.

Now, the condition of equilibrium of moments with respect to the load point is written as the following equation

$$\frac{ps}{4} = \int_0^{x_c} \sigma x b dx \tag{5}$$

Where x_c is the point where the softening is complete. Since the stress σ is the cohesive stress, so $\sigma = f(w)$. By substituting x as a function of w from (4), then

$$p = \frac{b}{s\theta^2} \int_0^{w_c} f(w) w dw \tag{6}$$

Where w_c is the opening displacement corresponding to x_c, i.e., $w(x_c) = w_c$. If the rotation is large enough, the displacement at the notch will be greater than the critical displacement,$w > w_C$, and the real crack will propagate.

In Eq. (6), the integral is the first-order moment of the softening curve, which is equal to the abscissa $\overline{w}$ of the center of gravity of the area enclosed by the curve and the axes times by this area, which is G_F. Therefore, if θ is written as $\theta = \frac{U}{\left(\frac{S}{2}\right)}$ Expression seven will be achieved.

$$p = \frac{bs}{4u^2} G_F \overline{w} \tag{7}$$

Therefore, Eq. (5) could be written as

$$p = \frac{A}{u^2} \text{ and } A = \frac{bs}{4} G_F \overline{w} \tag{8}$$

According to Fig. 4, "A" is a parameter determined by the least-square fitting of a straight line through the origin. It should be noted that in the p-u^{-2} diagram, the first stages of the horizontal axis represent the last stages of the beam fracture. In fact, when u increases, the u^{-2} parameter decreases with the square power. The curve fitting is applied on the first stage of the curve according to the proposed model for the final loading stage (Fig. 4).

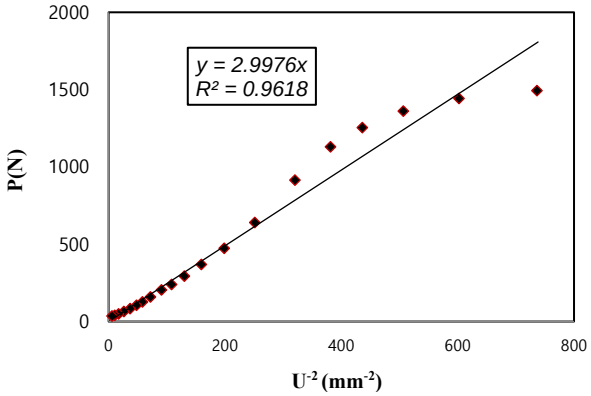

Fig. 4 Example of the determination of constant 'A' in Eq. (8) for a specific case

If it is assumed that there is perfect weight compensation, the value of $\overline{w}$ in terms of "A," is

$$\overline{w} = \frac{4A}{bsG_F} \tag{9}$$

Once $\overline{w}$ has been determined; It is a simple geometrical problem to define the bilinear softening curve.

Horizontal intercept, w_1, could be determined from the softening function, shown in Fig. 2, as Eq. (10).

$$w_1 = \frac{2G_f}{f_t} \tag{10}$$

Where the specific fracture energy G_f is the size-independent fracture energy, which is determined using the size-effect law. In this method, extrapolations are applied to the results of experiments on notched beams with different depths.

In addition, experimental relationships for finding W_1, independent of G_f, have been proposed by researchers, such as the proposed standard formula of CEB-FIP 1990 formula given in Eq. (1).

"W_c" is the critical crack opening, which could be obtained from the quadratic equation.

$$w_c^2 - w_c \frac{6\overline{w}\left(\frac{G_F}{f_t'}\right) - 2w_1\left(\frac{G_F}{f_t'}\right)}{2\left(\frac{G_F}{f_t'}\right) - w_1} + \frac{6\overline{w}w_1\left(\frac{G_F}{f_t'}\right) - 4w_1\left(\frac{G_F}{f_t'}\right)^2}{2\left(\frac{G_F}{f_t'}\right) - w_1} = 0 \tag{11}$$

and the coordinates of the kink point are given by

$$w_k = w_1 \frac{w_c - 2(\frac{G_F}{f_t'})}{w_c - w_1} \tag{12}$$

$$\sigma_k = f_t' \frac{2\left(\frac{G_F}{f_t'}\right) - w_1}{w_c - w_1} \tag{13}$$

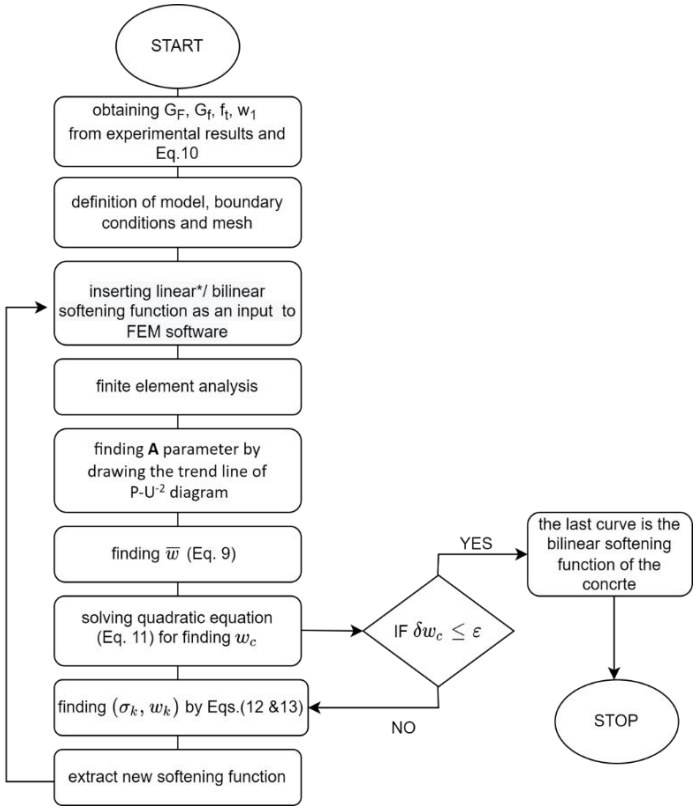

Fig. 5 flowchart of the proposed algorithm

*for the first iteration, a linear softening function can be used

Derivations of Eqs. (11) to (13) are given in appendix1. In this paper, a semi-automatic algorithm is proposed to find the bilinear cohesive stress function of the concrete utilizing ABAQUS software. According to Fig. 5, in each step, 'A' is determined by drawing the trend line $p - u^{-2}$ diagram, derived from finite element analysis. Afterward, the values of $\overline{w}$ and w_c are derived from Eq. (9) and Eq. (11), respectively. The coordinates of the kink point (σ_k, w_k) are found by Eq. (12) and Eq. (13). The process continues once the difference between two sequent critical displacements w_c becomes less than very small displacement, epsilon (ε). ε, in this research, is selected as 0.0001 mm.

The presented method provides precise responses in comparison with the results of experimental tests. Fig. 5 illustrates the flowchart of the proposed algorithm, explained previously, to find a softening function.

3. FEM modeling

Using non-linear fracture mechanics combined with numerical methods such as the finite element method (FEM) is inevitable for determining the actual response of concrete structures.

For numerical modelling, the concrete matrix is established, and the solid element (CPS4R) is

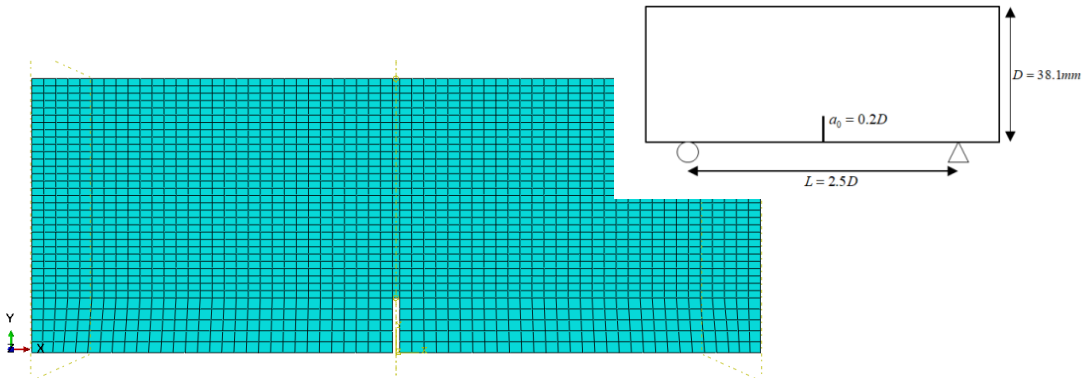

Fig. 6 The geometry of the beam and the finite element mesh (four nodes, plane stress elements)

assigned. Due to obtaining reliable results with less computational time, different element sizes for a couple of models were considered and compared together to evaluate the mesh sensitivity effect. Finally, the mesh size of 1.7 mm is distinguished to be the most suitable mesh size in this model (Fig. 6).

Conventional approaches to model fracture in concrete structures can be primarily grouped into discrete crack models (Abbasnia and Aslami 2015, Broujerdian *et al.* 2019), the orthotropic smeared-crack models (Rots and Blaauwendraad 1989, Hsu and Zhu 2002, Vecchio and Collins 1986, Broujerdian and Kazemi 2016), and the damage models (Ju 1989, Wu *et al.* 2006, Mazloom *et al.* 2019, Tesser *et al.* 2011, Feng *et al.* 2018, Faria *et al.* 1998, Lee and Fenves 1998).

The discrete crack model considers the crack as a geometric entity (ACI 446.3R-97 1997). In this approach, re-meshing after each step of crack propagation is carried out until the crack length would be developed completely unless the crack path was predetermined (Broujerdian *et al.* 2019). Concrete, in smeared crack models, is assumed as an orthotropic material, in which cracks are modeled by altering the constitutive (stress-strain) relations in the vicinity of cracks and are smeared over entire elements (ACI 446.3R-97 1997).

The significant advantage of the smeared crack model is its simplicity, but also, there is a severe objection against these models.

The result of calculations made with the smeared crack model depends on the choice of mesh; nevertheless, an alternative approach is proposed by damage mechanics to make the concrete constitutive model. Concrete damage plasticity, CDP, lies in the continuum, plasticity, and the concrete damage, integrated into a framework for analyzing the concrete structures (Wu *et al.* 2006, Tesser *et al.* 2011). Having considered the aforementioned advantages of CDPM, this approach has been used for modelling the beams in this study.

Material degradation is indicated by an internal variable, i.e., the damage. By adjusting the laws for the evolution of damage, the conventional properties of concrete materials can be simulated.

The total strain is divided into two parts. Hence, it is possible to represent the nonlinearity and irreversible deformation of the concrete based on elastic-plastic theory.

$$\varepsilon = \varepsilon^{el} + \varepsilon^{pl} \tag{14}$$

In which, $\varepsilon^{el}$and ε^{pl} are the elastic and plastic strains, respectively. CDP model provides a scalar damage variable, d, to consider the progressive material damage. It can take values from

zero to one (Abaqus 2013). The stress state function is as below.

$$\sigma_{ij} = (1-d)D_{ijkl}^{el}\left(\varepsilon_{ij} - \varepsilon_{ij}^{pl}\right) \tag{15}$$

In which D_{ijkl}^{el} is the initial elasticity matrix, ε_{ij} is the strain tensor, and ε_{ij}^{pl} is the plastic strain tensor.

For uniaxial monotonic loading conditions, the variable d can be replaced by d_c and d_t, which represent damage in compression and tension, respectively. Consequently, Eq. (15) can be simplified into

$$\sigma_c = (1-d_c)E_0\left(\varepsilon_c - \varepsilon_c^{pl}\right) \tag{16}$$

$$\sigma_t = (1-d_t)E_0\left(\varepsilon_t - \varepsilon_t^{pl}\right) \tag{17}$$

Where E_0 is the initial elastic modulus.

To use CDPM in finite element modelling, it is necessary to determine the damage evolution and material degradation. Due to the incomprehensive understanding of the concrete failure phenomenon, there is no quantitative relationship between stress conditions and concrete degradations. Thus, empirical formulations have been proposed to predict the damage evolution (Xu and Sugiura 2013, Wang *et al.* 2014, Fang *et al.* 2013, Lu *et al.* 2009, Pavlovic *et al.* 2013, Pan *et al.* 2015, Xu *et al.* 2014, Yan *et al.* 2016). Some of these formulations are based on a simple assumption that the non-linear behavior of concrete before reaching peak stress (σ_0) is only owing to plasticity, while Softening after the peak stress is caused only by damage. Consequently, for simplicity, the variable d is defined as a linear function of the stress in the softening region (σ^*) as in the following equation (Pavlovic *et al.* 2013)

$$d = 1 - \frac{\sigma^*}{\sigma_0} \tag{18}$$

4. Results and discussion

The proposed algorithm was validated by the results of the three-point beam bending (TPB) tests for different concrete mixtures, reported by Afzali-Naniz and Mazloom (2019). Self-compacting lightweight concrete (SCLC) is categorized as high-performance concrete. The design of the mixtures is detailed in Table 2.

Table 3 presents the mechanical properties such as tensile strength (f_t'), compressive strength (f_c), and the modulus of elasticity (E) and fracture parameters of the SCSLC containing colloidal Nano-silica (Afzali-Naniz and Mazloom 2019).

Based on the fracture parameters, the proposed softening model predicts the load-deflection curves for the different concrete mixtures.

Fig. 7(a-d) demonstrates the agreements between numerical predictions and the concrete mixtures' experimental results. It is very promising that the model proposed in this paper can predict maximum load with high accuracy.

As shown in Fig. 7 and Table 4, the Hillerborg linear model predicts maximum load much more than the experimental peak load. Moreover, by using the Hillorborg linear model as an input in FEM software, it is impossible to predict the softening response of concrete specimens precisely.

Table 2 Mixture proportions of SCLC (Afzali-Naniz and Mazloom 2019)

Materials	Weight (kg/m^3)			
	Mix. 1	Mix. 2	Mix. 3	Mix. 4
Colloidal Nano-silica (CS) (%)	0	1	3	4
Cement (C)	450	445.5	436.5	427.5
Sand	800	800	800	800
LECA	270	270	270	270
Limestone powder	230	230	230	230
Free water	157.5	157.5	157.5	157.5
Super Plasticizer	9	9.45	11.7	13.5
w/b	0.35	0.35	0.35	0.35

Table 3 Fracture parameters and the mechanical properties of matrix (Afzali-Naniz and Mazloom 2019)

Mixtures	Mix. 1	Mix. 2	Mix. 3	Mix. 4
$f_c(Mpa)$	39.35	43.8	46.9	46
$f_t'(Mpa)$	3.05	3.3	3.6	3.58
$E(Gpa)$	23.05	24.7	25.9	25.45
a_0/d	0.2	0.2	0.2	0.2
$G_f(\frac{N}{m})$	33.98	38.3	42.6	39.75
$G_F(\frac{N}{m})$	80.9	88.09	93.45	91.43
$CTOD_c$	0.0183	0.0203	0.0217	0.0204

Table 4 Peak loads obtained from numerical simulations and experimental data

	Experimental Data (Afzali-Naniz 2019)	Numerical prediction				
		Proposed algorithm	(Hillerborg,1976)	(Petersson1981)	(CEB 1990)	(Park 2008)
Mix. 1	1393	1391.4	1500.47	1465.76	1470.98	1378.16
Mix. 2	1396	1395.12	1500.43	1471.33	1480.74	1392.12
Mix. 3	1513	1512.16	1859.54	1704.93	1717.21	1510.99
Mix. 4	1502	1495.47	1845.25	1679.52	1598.27	1481.47

Thus, the use of linear models of softening function in simulating concrete structures is highly error-prone in predicting the peak load and fracture behavior of concrete.

As is evident from numerical simulation, the definition of the softening function has a vital role in predicting peak load and concrete fracture behavior. The peak load was obtained from finite element modelling using the softening curve proposed in this paper, and the proposed bilinear curves of Petersson (1981), CEB-FIP Model Code, and Park *et al.* (2008) are compared in Table 4. Fig. 8 shows the softening curves obtained from the proposed algorithm compared to the other softening curves presented in the literature for different mixtures.

It is clear that the proposed bilinear models have better predictions than linear curves. Contrary

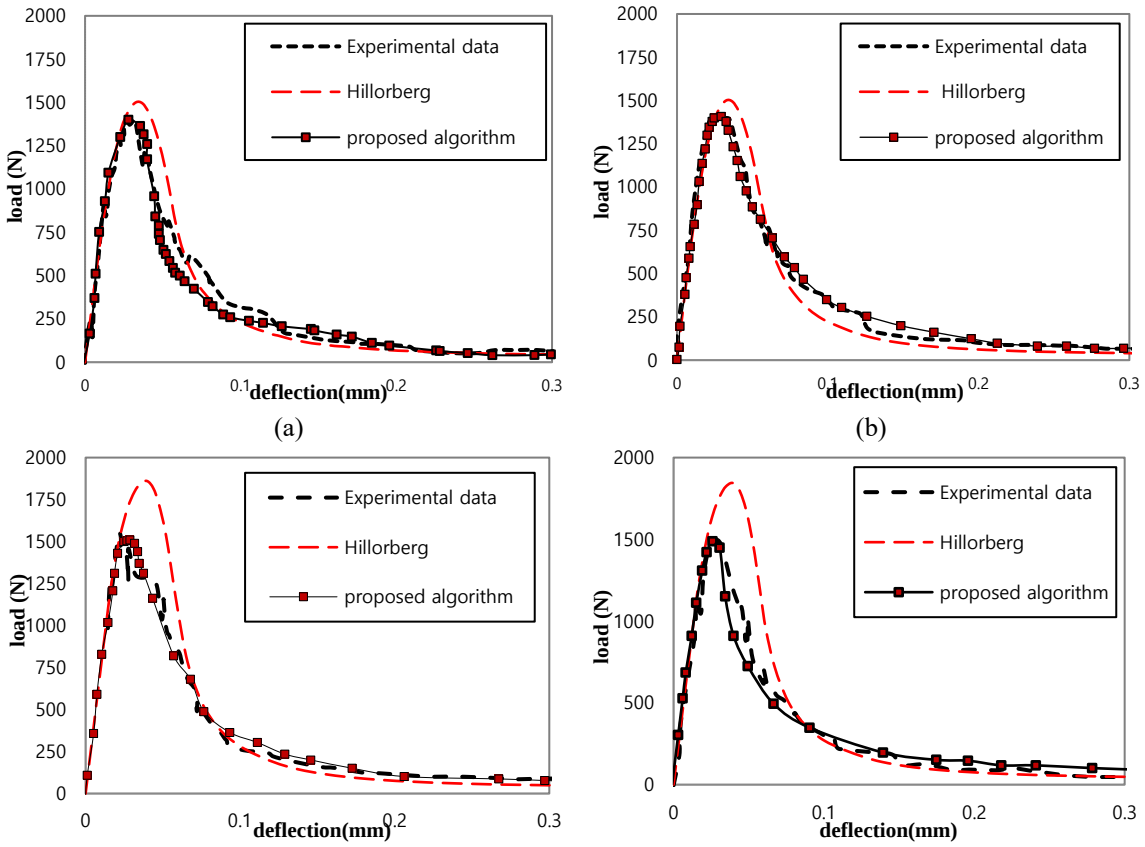

Fig. 7 Numerical predictions of load-deflection curves compared with experimental data (a) Mix. 1, (b) Mix. 2, (c) Mix. 3, (d) Mix. 4

Table 5 Characteristics of softening models obtained from the proposed algorithm

	N*	A parameter	$w_1(mm)$	$w_c(mm)$	$w_k(mm)$	σ_k
			$\times 10^{-2}$			
Mix. 1	8	2.9976	2.23	17.22	1.779	61.48
Mix. 2	11	3.5636	2.32	21.16	1.950	52.83
Mix. 3	7	3.2352	2.37	19.56	1.977	59.14
Mix. 4	5	3.2751	2.22	19.47	1.849	59.90

*Number of iteration

to the proposed model in this article, linear models estimate the peak loads up to ten percent higher than the experimental peak loads. The proposed method in this paper seems to have excellent capability and accuracy for use in finite element modelling to simulate concrete elements. Fig. 9 illustrates the crack propagation in the depth of the beam, which matches the shape of the crack in the laboratory specimen. The coordinates of the bilinear curves obtained from the proposed

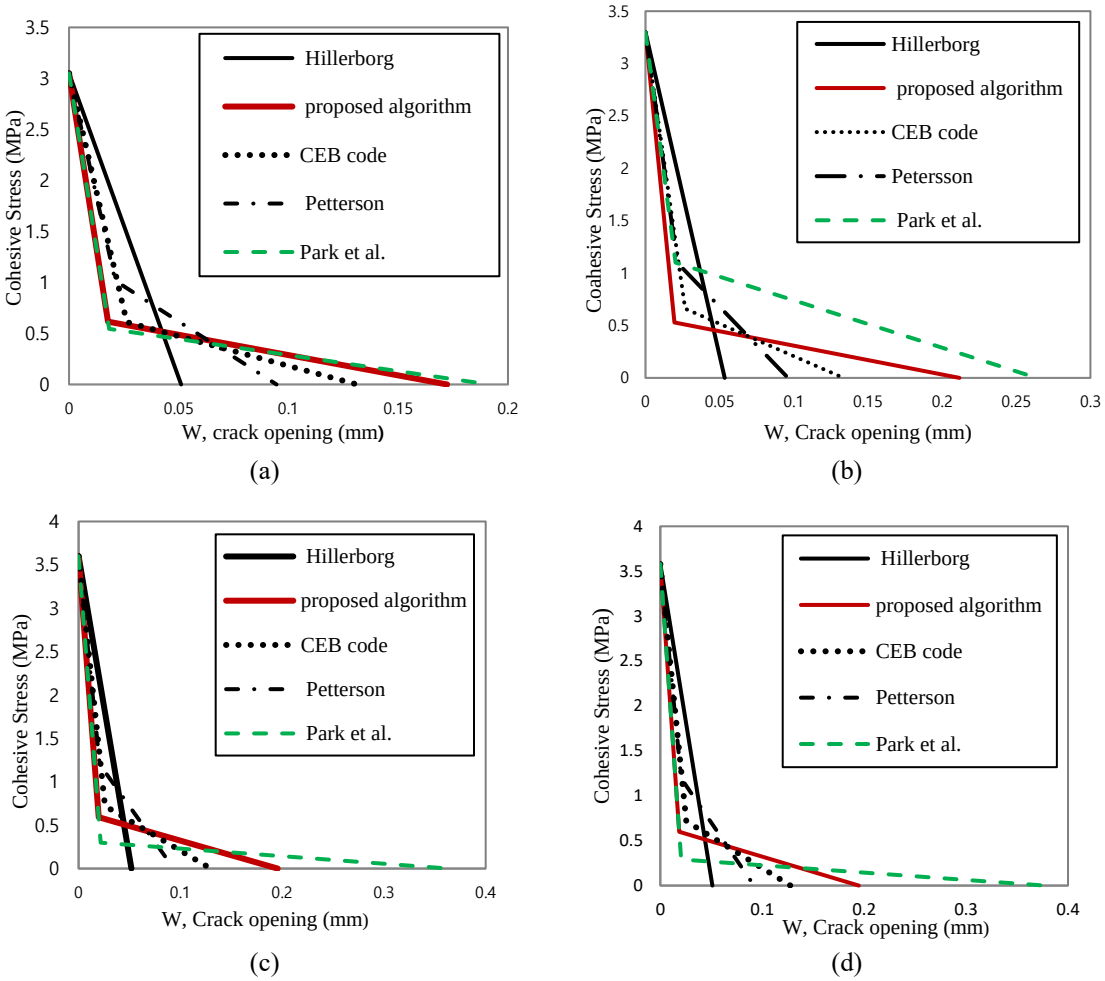

Fig. 8 The softening curves used in the FEM for comparison (a) Mix. 1, (b) Mix. 2, (c) Mix. 3 and (d) Mix. 4

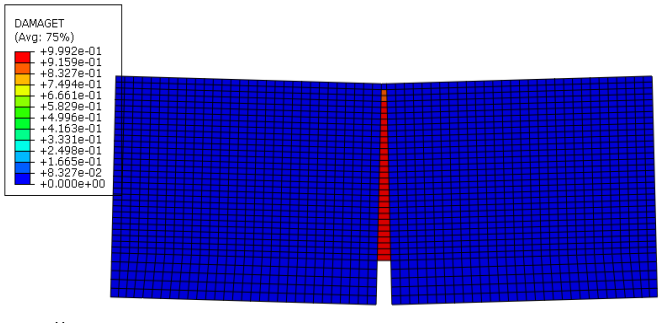

Fig. 9 Crack propagation in the depth of the beam

algorithm for different mixtures are given in Table 5. The N parameter is the number of iterations made to achieve convergence in this table.

Table 6 comparison between the double-k fracture parameters derived from experimental and proposed algorithm results

	initial cracking toughness, K_{IC}^{ini}		unstable fracture toughness, K_{IC}^{un}	
	Experimental results	FEM analysis using the proposed algorithm	Experimental results	FEM analysis using the proposed algorithm
Mix. 1	0.338	0.337	0.829	0.828
Mix. 2	0.339	0.339	0.836	0.835
Mix. 3	0.368	0.367	0.884	0.884
Mix. 4	0.365	0.363	0.890	0.887

To validate the proposed method at different loading stages with more accuracy, the results of double-k fracture toughness taken from the finite element (FEM) analysis and the experiment are compared in Table 6. According to the double-k fracture model, two size-independent criteria entitled as initial cracking toughness K_{IC}^{ini} and unstable fracture toughness K_{IC}^{un} can predict different stages of the concrete fracture process. Initial toughness K_{IC}^{ini} is defined as the inherent toughness of a material and is calculated directly by the initial crack load P^{ini} and the initial notch a_0 using the linear elastic fracture mechanics (LEFM). Unstable crack toughness K_{IC}^{un} can be obtained with the peak load P_u and the effective crack length using the same LEFM formula, which indicates the beginning of unstable crack propagation. For an elastic concrete beam with a total height D, notch length a_0, thickness B, and span length S, the deflection and the stress intensity factor (SIF) are written as

$$\delta_i = \frac{P_i}{4BE}\left(\frac{S}{D}\right)^3\left[1+\frac{5W_gS}{8P_i}+\left(\frac{D}{S}\right)^2\left\{2.70+1.35\frac{W_gS}{P_i}\right\}-0.84\left(\frac{D}{S}\right)^3\right] + \frac{9P_i}{2BE}\left(1+\frac{W_gS}{2P_i}\right)\left(\frac{S}{D}\right)^2 F_2(\alpha_0) \tag{19}$$

$$F_2(\alpha_0) = \int_0^{\alpha_0} \beta F^2(\beta)\, d\beta \tag{20}$$

$$K_I = \sigma_N \sqrt{a} F(\alpha) \tag{21}$$

Where $\alpha = \frac{a}{D}, \alpha_0 = \frac{a_0}{D}$, and $F(\alpha)$ is the geometric factor which depends on the S/D ratio of the beam. The term W_g is the self-weight of the beam per unit length. P_i is the elastic force corresponding to the elastic deflection δ_i of the concrete beam with the elastic modulus of E. Moreover, σ_N is the nominal stress of the beam with the "a" crack length (Kumar and Barai 2011). As shown in Table 6, there is a good consistency between the results of the double-k parameters derived from the experimental results and the FEM analysis, which indicates the strength of the proposed algorithm in predicting concrete behavior at different fracture stages (i.e., crack initiation, stable and unstable crack propagation).

Concrete load-displacement curves have different zones, as shown in Fig. 10. The curve initially behaves linearly from zero to p2. After p2, the initial micro-cracks that existed before loading in the cement paste aggregate interface begin to grow. This non-elastic phase continues

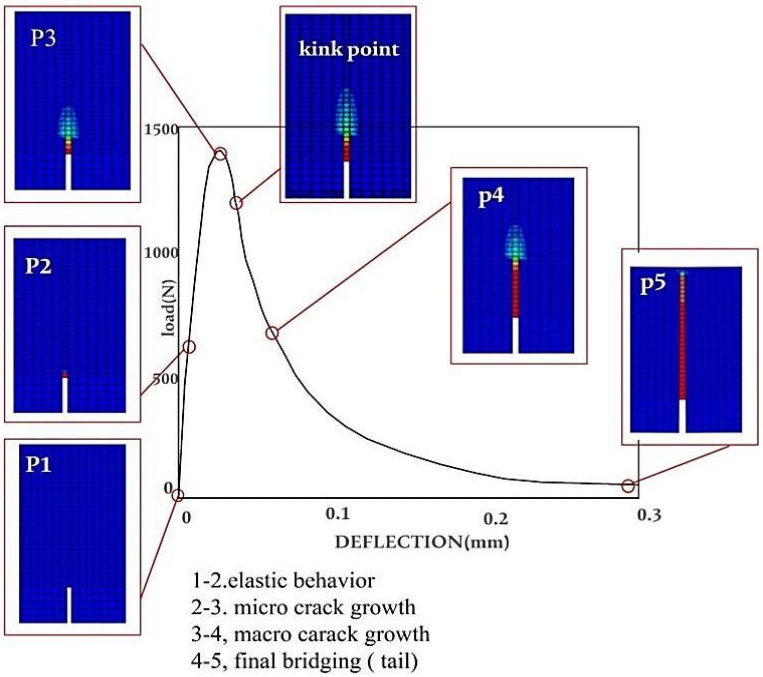

Fig. 10 Load-deflection curve of the concrete beam (Mix. 2)

until it reaches the ultimate loading capacity of the specimen, known as the peak load (p3).

After (p3), the specimen is damaged and fractured due to the micro-crack coalescence, and the curve shows a downward trend (p4 & p5). As the curve descends, the micro-cracks become unstable, and localized cracking occurs over a narrow area of micro cracks, termed as the fracture process zone (FPZ).

With increasing displacement, since concrete is a quasi-brittle material, micro-cracks become macro-cracks.

As shown in Fig. 11, the beam initially has elastic behavior. In Fig. 11, p2b to p5b, the stress profile in the notched beam can be seen. The notched beam's opening displacement and stress distribution in Fig. 11 correspond to loads and deflections in Fig. 10.

With increasing the load in the beam, when the tensile stress reaches the cracking stress in the furthest tensile fiber, the crack is localized, and as the load increases, the length of the fictitious crack increases. In Fig. 11, p3c, p4c, and p5c show the rise in tension damage, which means crack propagation. When the crack opening reaches its critical value w_c, the real crack begins to propagate. The crack can no longer transfer stresses at this stage (p5).

The softening curve can be reproduced again using the stress output and crack opening output. Fig. 12 illustrates the Position of the points at the top of the notch (x=0) on the tensile stress-strain curve and the bilinear softening curve. According to Fig. 12, at p1 and p2, the cohesive stress is zero, and the stress-strain relationship is linear.

The p3 is on the steepest part of the bilinear curve.

The kink point occurs after the peak load on the softening branch of the load-displacement curve. The p4 is located on the shallow tail of the bilinear curve. Because $w \geq w_c$ at p5, the cohesive stress is zero.

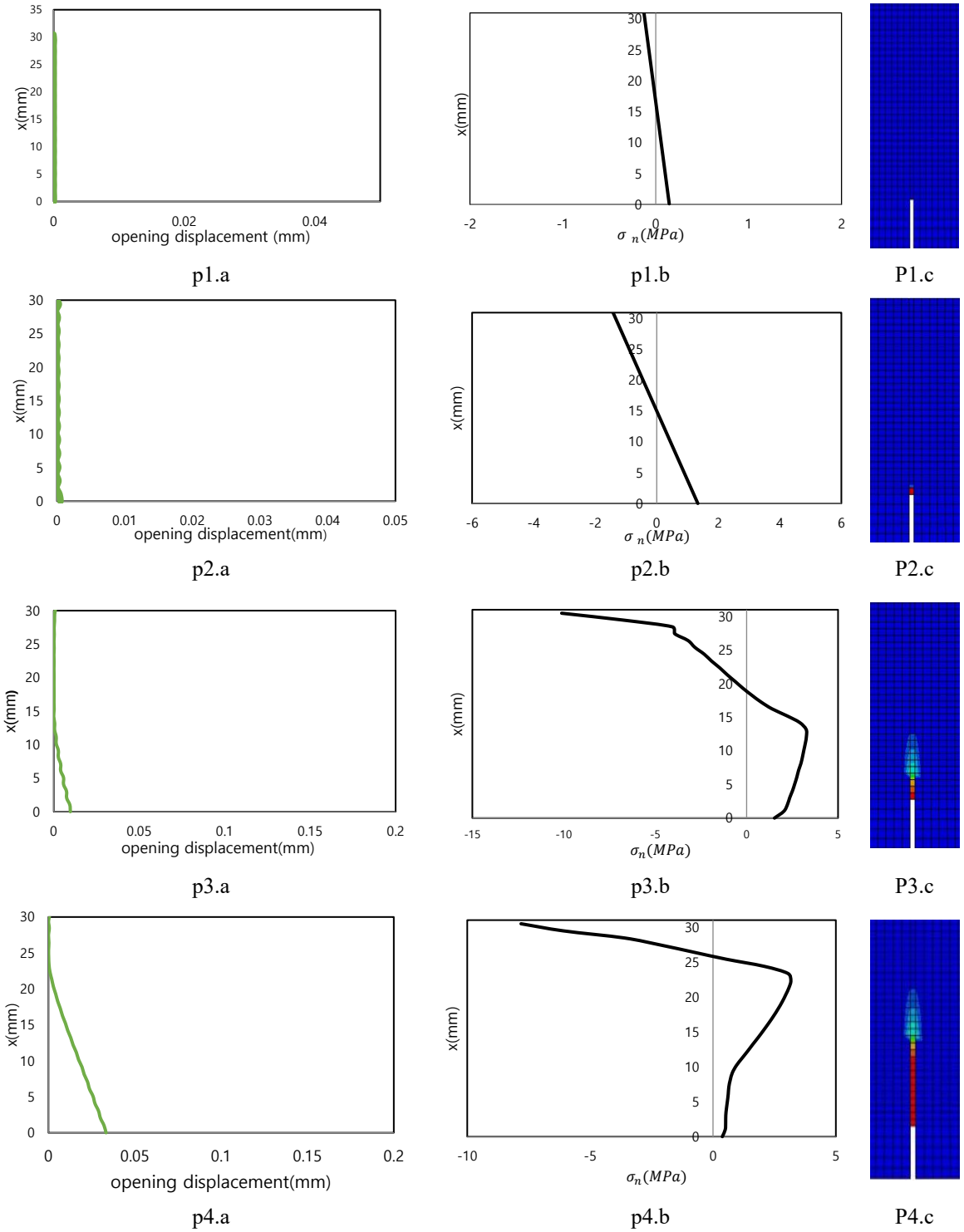

Fig. 11. (a) Distribution of the opening displacement in the depth of the beam, (b) Stress distribution in the notched beam (c) Tension damage in the notched beam

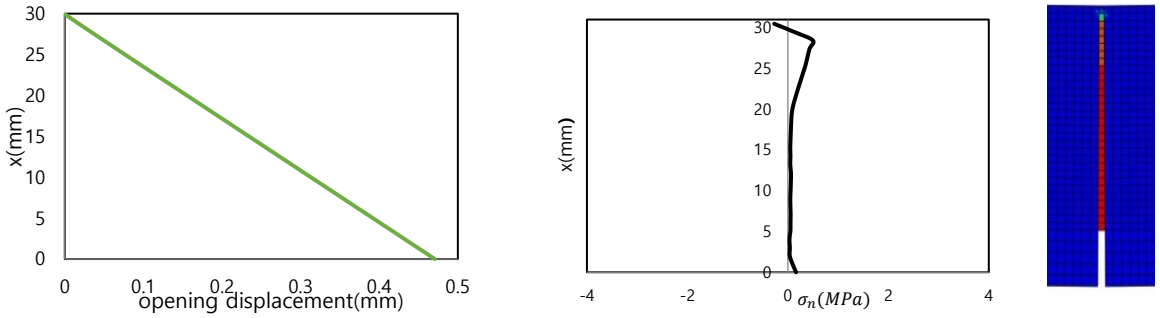

p5.a p5.b p5.c

Fig. 11. Continued

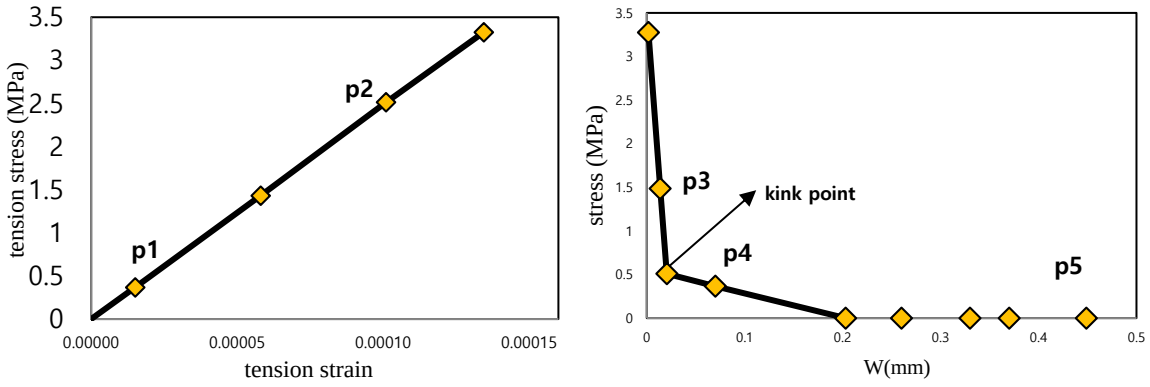

(a) (b)

Fig. 12 Position of the desired points at x=0 on the (a) Tensile stress-strain curve (b) Bilinear softening curve

As shown from Fig. 10 and Fig. 12, the kink point occurs in the $0.8p_{peak}$, at the softening branch of the load-displacement diagram. This indicates that the long tail of the softening curve corresponds to the softening part of the load-deflection curve, which is predicted precisely by the proposed algorithm.

Moreover, it is inferred from the results that FPZ established itself entirely at the notch tip after the loading reached its peak load and in the softening branch of the load-displacement curve (Figs. 11, 12).

5. Conclusions

The research described in this paper presents a novel inverse algorithm for predicting the softening function of concrete. This algorithm is based on the kinematics of the beams at the late stages of the loading. The motivation behind this study is that determining the softening functions is the primary and effective part of the cohesive crack model of the concrete. The parameters required for this algorithm can be obtained with the help of Common fracture tests. Actually, by

this algorithm and finite element analysis, the exact softening curve of concrete can be found. In fact, the finite element results of the notched beams led to numerical results that were in excellent agreement with the experimental peak loads and load-displacement curves of the specimens with different concrete mixtures. In addition, the fracture parameters derived from experimental results and the finite element analysis using the proposed algorithm were well consistent. It means that the presented algorithm can considerably reduce the number of tests to find the fracture behavior of concrete elements.

References

Abaqus. (2013), Abaqus 6.13 Analysis User's Guide, Dassault Systèmes.

Abbasnia, R. and Aslami, M. (2015), "Numerical simulation of concrete fracture under compression by explicit discrete element method", *Int. J. Civil Eng.*, **13**(3), 245-254. https://doi.org/10.22068/IJCE.13.3.245.

Abna, A. and Mazloom, M. (2022), "Flexural properties of fiber reinforced concrete containing silica fume and nano-silica", *Mater. Lett.*, **316**, 132003. https://doi.org/10.1016/j.matlet.2022.132003.

ACI 446.3R-97 (1997), Finite Element Analysis of Fracture in Concrete Structures, American Concrete Institute, Farmington Hills, USA.

Afzali-Naniz, O. and Mazloom, M. (2019), "Fracture behavior of self-compacting semi-lightweight concrete containing nano-silica", *Adv. Struct. Eng.*, **22**(10), 2264-2277. https://doi.org/10.1177/1369433219837426.

Alam, S.Y. and Loukili, A. (2020), "Effect of micro-macro crack interaction on softening behaviour of concrete fracture", *Int. J. Solid. Struct.*, **182**, 34-45. https://doi.org/10.1016/j.ijsolstr.2019.08.003.

ASTM C 469/C 496M. (2004), Standard Test Method for Splitting Tensile Strength of Cylindrical Concrete Specimens, ASTM International.

ASTM Standard C469. (2002), Standard Test Method for Static Modulus of Elasticity and Poisson' s Ratio of Concrete in Compression, ASTM International 04: 1-5.

Barenblatt, G.I. (1962), "The mathematical theory of equilibrium cracks in brittle fracture", *Adv. Appl. Mech.*, **7**, 55-129. https://doi.org/10.1016/S0065-2156(08)70121-2.

Bazant, Z.P. (2003), "Fracture mechanics of concrete: Concepts, models and determination of material properties", *FractureMechanics of Concrete Structures*, 25-44.

Bazant, Z.P. (2001), "Concrete fracture models: testing and practice", *Eng. Fract. Mech.*, **69**(2), 165-205. https://doi.org/10.1016/S0013-7944(01)00084-4.

Bazant, Z.P. and Phillip A.P. (1987), "Determination of fracture energy from size effect and brittleness number", *ACI Mater. J.*, **84**(6), 463-80. https://doi.org/10.14359/2526.

Bažant, Z.P. and Planas, J. (2019), *Fracture and Size Effect in Concrete and Other Quasibrittle Materials*, Routledge, New York, NY, USA.

Bhosale, A.B., Lakavath, C. and Prakash, S.S. (2020), "Multi-linear tensile stress-crack width relationships for hybrid fibre reinforced concrete using inverse analysis and digital image correlation", *Eng. Struct.*, **225**, 111275. https://doi.org/10.1016/j.engstruct.2020.111275.

Broujerdian, V., Karimpour, H. and Alavikia, S. (2019), "Predicting the shear behavior of reinforced concrete beams using non-linear fracture mechanics", *Int. J. Civil Eng.*, **17**(5), 597-605. https://doi.org/10.1007/s40999-018-0336-6.

Broujerdian, V., Sherafati, A. and Karimpour, H. (2018), "Effect of crack cohesive stresses on the load-deformation response of reinforced concrete beams", *Amirkabir J. Civil Eng.*, **50**(1), 89-96. https://doi.org/10.22060/ceej.2017.11366.5012.

Broujerdian, V. and Kazemi, M.T. (2016), "Non-linear finite element modeling of shear-critical reinforced concrete beams using a set of interactive constitutive laws", *Int. J. Civil Eng.*, **14**(8), 507-519.

https://doi.org/10.1007/s40999-016-0024-3.
Ceb-Fip, Model Code (1990), Design Code, Comite Euro International Du Beton, 51-59.
Dugdale, D.S. (1960), "Yielding of steel sheets containing slits", *J. Mech. Phys. Solid.*, **8**(2), 100-104. https://doi.org/10.1016/0022-5096(60)90013-2.
Fang, X.D., Jiang, B., Wei, H., Zhou, Y., Jiang, Y. and Lai, H. (2013), "Axial compressive test and study on steel tube confined high strength concrete shear wall", *J. Build. Struct.*, **34**(3), 100-109.
Faria, R., Oliver, J. and Cervera, M. (1998), "A strain-based plastic viscous-damage model for massive concrete structures", *Int. J. Solid. Struct.*, **35**(14), 1533-58. https://doi.org/10.1016/S0020-7683(97)00119-4.
Feng, D.C., Ren, X.D. and Li, J. (2018), "Softened damage-plasticity model for analysis of cracked reinforced concrete structures", *J. Struct. Eng.*, **144**(6), 04018044. https://doi.org/10.1061/(ASCE)ST.1943-541X.0002015.
Gao, D., Ding, C., Pang, Y. and Chen, G. (2021), "An inverse analysis method for multi-linear tensile stress-crack opening relationship of 3D/ 4D/ 5D steel fiber reinforced concrete", *Constr. Build. Mater.*, **309**, 125074. https://doi.org/10.1016/j.conbuildmat.2021.125074.
Guinea, G.V., Planas, J. and Elices, M. (1994), "A general bilinear fit for the softening curve of concrete", *Mater. Struct.*, **27**(2), 99-105. https://doi.org/10.1007/BF02472827.
Gustafsson, P.J. and Hillerborg, A. (1985), "Improvements in concrete design achieved through the application of fracture mechanics", *NATO ASI Series, Series E: Appl. Sci.*, **94**, 667-680. https://doi.org/10.1007/978-94-009-5121-1_24.
Hillerborg, A., Modéer, M. and Petersson, P.E. (1976), "Analysis of crack formation and crack growth in concrete by means of fracture mechanics and finite elements", *Cement Concrete Res.*, **6**(6), 773-781. https://doi.org/10.1016/0008-8846(76)90007-7.
Hsu, T.T. and Zhu, R.R. (2002), "Softened membrane model for reinforced concrete elements in shear", *Struct. J.*, **99**(4), 460-469. https://doi.org/10.14359/12115.
Ju, J.W. (1989), "On energy-based coupled elastoplastic damage theories: Constitutive modeling and computational aspects", *Int. J. Solid. Struct.*, **25**(7), 803-833. https://doi.org/10.1016/0020-7683(89)90015-2.
Karamloo, M. and Mazloom, M. (2018), "An efficient algorithm for scaling problem of notched beam specimens with various notch to depth ratios", *Comput. Concrete*, **22**(1), 39-51. https://doi.org/10.12989/cac.2018.22.1.039.
Karimpour, H. and Mazloom, M. (2022), "Pseudo-strain hardening and mechanical properties of green cementitious composites containing polypropylene fibers", *Struct. Eng. Mech.*, **81**(5), 575-589. https://doi.org/10.12989/sem.2022.81.5.575.
Kumar, S. and Barai, S.V. (2011), *Concrete Fracture Models and Applications*, Springer Berlin, Heidelberg.
Lee, J. and Fenves, G.L. (1998), "Plastic-damage model for cyclic loading of concrete structures", *J. Eng. Mech.*, **124**(8), 892-900. https://doi.org/10.1061/(ASCE)0733-9399(1998) 124:8(892).
Li, V.C., Chan, C.M. and Leung, C.K. (1987), "Experimental determination of the tension-softening relations for cementitious composites", *Cement Concrete Res.*, **17**(3), 441-52. https://doi.org/10.1016/0008-8846(87)90008-1.
Lu, X.Z., Ye, L.P. and Miao, Z.W. (2009), "Elasto-plastic analysis of buildings against earthquake", *China Architecture and Building Press*, Beijing.
Mazloom, M., Karimpanah, H. and Karamloo, M. (2020), "Fracture behavior of monotype and hybrid fiber reinforced self-compacting concrete at different temperatures", *Adv. Concrete Constr.*, **9**(4), 375-386. https://doi.10.12989/acc.2020.9.4.375.
Mazloom, M., Pourhaji, P. and Afzali Naniz, O. (2021), "Effects of halloysite nanotube, nano-silica and micro-silica on rheology, hardened properties and fracture energy of SCLC", *Struct. Eng. Mech.*, **80**(1), 91-101. https://doi.org/10.12989/sem.2021.80.1.091.
Mazloom, M., Pourhaji, P., Shahveisi, M. and Jafari, S.H. (2019), "Studying the Park-Ang damage index of reinforced concrete structures based on equivalent sinusoidal waves", *Struct. Eng. Mech.*, **72**(1), 845-859. https://doi.org/10.12989/sem.2019.72.1.083.

Mazloom, M. and Mirzamohammadi, S. (2019), "Thermal effects on the mechanical properties of cement mortars reinforced with aramid, glass, basalt and polypropylene fibers", *Adv. Mater. Res.*, **8**(2),137-154. https://doi.org/10.12989/amr.2019.8.2.137.

Mazloom, M. and Mirzamohammadi, S. (2021a), "Fracture of fibre-reinforced cementitious composites after exposure to elevated temperatures", *Mag. Concrete Res.*, **73**(14), 701-713. https://doi.org/10.1680/jmacr.19.00401.

Mazloom, M. and Mirzamohammadi, S. (2021b), "Computing the fracture energy of fiber-reinforced cementitious composites using response surface methodology", *Adv. Comput. Des.*, **6**(3), 225-239. https://doi.org/10.12989/acd.2021.6.3.225.

Mehta, P.K. and Monteiro, P.J. (2017), *Concrete Microstructure, Properties and Materials*, McGraw-Hill Education.

Van Mier, J.G.M. (1986), "Fracture of concrete under complex stress", *Heron*, **31**(3), 1-90.

Miller, R.A., Castro-Montero, A. and Shah, S.P. (1991), "Cohesive crack models for cement mortar examined using finite-element analysis and laser holographic measurements", *J. Am. Ceram. Soc.*, **74**(1), 130-138. https://doi.org/10.1111/j.1151-2916.1991.tb07308.x.

Østergaard, L., Lange, D. and Stang, H. (2004), "Early-age stress-crack opening relationships for high performance concrete", *Cement Concrete Compos.*, **26**(5), 563-72. https://doi.org/10.1016/S0958-9465(03)00074-X.

Pan, Z., Wu, C., Liu, J., Wang, W. and Liu, J. (2015), "Study on mechanical properties of cost-effective polyvinyl alcohol engineered cementitious composites (PVA-ECC)", *Constr. Build. Mater.*, **78**, 397-404. https://doi.org/10.1016/j.conbuildmat.2014.12.071.

Park, K., Paulino, G.H. and Roesler, J.R. (2008), "Determination of the kink point in the bilinear softening model for concrete", *Eng. Fract. Mech.*, **75**(13), 3806-3818. https://doi.org/10.1016/j.engfracmech.2008.02.002.

Pavlovic, M.N. (1996), "Fracture mechanics of concrete: Applications of fracture mechanics to concrete, rock and other quasi-brittle materials", *Eng. Struct.*, **18**(11), 887-888. https://doi.org/10.1016/0141-0296(96)84816-4.

Pavlović, M., Marković, Z., Veljković, M. and Buđevac, D. (2013), "Bolted shear connectors vs. headed studs behaviour in push-out tests", *J. Constr. Steel Res.*, **88**, 134-149. https://doi.org/10.1016/j.jcsr.2013.05.003.

Petersson, P.E. (1981), "Crack growth and development of fracture zones in plain concrete and similar materials", Report No. LUTVDG/TVBM--1006/1-174/(1981); Lund Institute of Technology, Division of Building Materials.

Reddy, K.C. and Subramaniam, K.V. (2017), "Analysis for multi-linear stress-crack opening cohesive relationship: Application to macro-synthetic fiber reinforced concrete", *Eng. Fract. Mech.*, **169**, 128-145. https://doi.org/10.1016/j.engfracmech.2016.11.015.

Reinhardt, H.W., Cornelissen, H.A. and Hordijk, D.A. (1986), "Tensile tests and failure analysis of concrete", *J. Struct. Eng.*, **112**(11), 2462-2477. https://doi.org/10.1061/(ASCE)0733-9445(1986)112:11(2462).

RILEM, D.R. (1985), "Determination of the fracture energy of mortar and concrete by means of three-point bend tests on notched beams", *Mater. Struct.*, **18**(106), 285-290.

RILEM, TC89. (1990), "89-FMT, fracture mechanics of concrete-test methods, size-effect method for determining fracture energy and process zone size of concrete", *Mater. Struct.*, **23**, 461-465.

Rots, J.G. and Blaauwendraad, J. (1989), "Crack models for concrete: Discrete or smeared? Fixed multi-directional or rotatin?", *Heron*, **34**(1), 3-59.

Salehi, H. and Mazloom, M. (2019a), "Effect of magnetic-field intensity on fracture behaviors of self-compacting lightweight concrete", *Mag. Concrete Res.*, **71**(13), 665-679. https://doi.org/10.1680/jmacr.17.00418.

Salehi, H. and Mazloom, M. (2019b), "An experimental investigation on fracture parameters and brittleness of self-compacting lightweight concrete containing magnetic field treated water", *Arch. Civil Mech. Eng.*, **19**(3), 803-819. https://doi.10.1016/j.acme.2018.10.008.

Shah, S.P. (1990), "Experimental methods for determining fracture process zone and fracture parameters", *Eng. Fract. Mech.*, **35**(1-3), 3-14. https://doi.org/10.1016/0013-7944(90)90178-J.

Shi, Z. (2009), *Crack Analysis in Structural Concrete: Theory and Applications*, Butterworth-Heinemann.

Tesser, L., Filippou, F.C., Talledo, D.A., Scotta, R. and Vitaliani, R. (2011), "Nonlinear analysis of R/C panels by a two parameter concrete damage model", *ECCOMAS Thematic Conference: 3rd International Conference on Computational Methods in Structural Dynamics and Earthquake Engineering: An IACM Special Interest Conference, Programme*, Corfu, Greece, May.

Vecchio, F.J. and Collins, M.P. (1986), "The modified compression-field theory for reinforced concrete elements subjected to shear", *ACI J.*, **83**(2), 219-231. https://doi.org/10.14359/10416.

Wang, X., Su, Y. and Yan, L. (2014), "Experimental and numerical study on steel reinforced high-strength concrete short-leg shear walls", *J. Constr. Steel Res.*, **101**, 242-253. https://doi.org/10.1016/j.jcsr.2014.05.015.

Wittmann, F.H., Roelfstra, P.E., Mihashi, H., Huang, Y.Y., Zhang, X.H. and Nomura, N. (1987), "Influence of age of loading, water-cement ratio and rate of loading on fracture energy of concrete", *Mater. Struct.*, **20**(2), 103-110. https://doi.org/10.1007/BF02472745.

Wittmann, F.H., Rokugo, K., Brühwiler, E., Mihashi, H. and Simonin, P. (1988), "Fracture energy and strain softening of concrete as determined by means of compact tension specimens", *Mater. Struct*, **21**(1), 21-32. https://doi.org/10.1007/BF02472525.

Wu, J.Y., Li, J. and Faria, R. (2006), "An energy release rate-based plastic-damage model for concrete", *Int. J. Solid. Struct.*, **43**(3-4), 583-612. https://doi.org/10.1016/j.ijsolstr.2005.05.038.

Xu, C. and Sugiura, K. (2013), "FEM analysis on failure development of group studs shear connector under effects of concrete strength and stud dimension", *Eng. Fail. Anal.*, **35**, 343-354. https://doi.org/10.1016/j.engfailanal.2013.02.023.

Xu, X., Liu, Y. and He, J. (2014), "Study on mechanical behavior of rubber-sleeved studs for steel and concrete composite structures", *Constr. Build. Mater.*, **53**, 533-546. https://doi.org/10.1016/j.conbuildmat.2013.12.011.

Yan, J.B., Qian, X., Liew, J.R. and Zong, L. (2016), "Damage plasticity based numerical analysis on steel-concrete-steel sandwich shells used in the Arctic offshore structure", *Eng. Struct.*, **117**, 542-559. https://doi.org/10.1016/j.engstruct.2016.03.028.

Yon, J.H. (1995), "Comparisons of concrete fracture models", *KSCE J. Civil Environ. Eng. Res.*, **15**(3), 583-583. https://doi.org/10.1061/(ASCE)0733-9399(1997) 123:3(196).

CC

Appendix1.derivations of formulas

The derivations of Eq. (11) to Eq. (13) are as follows.

A. Finding w_k and σ_k

The area below the bilinear curve is equal to G_F. By writing the area below the bilinear curve in terms of σ_k and equating it withG_F, Eq. (A.1) is found.

$$G_F = \frac{W_1 f_t}{2} + \frac{\sigma_k (w_c - w_1)}{2} \tag{A.1}$$

By rearranging Eq. (A.1), σ_k is found as Eq. (A.2).

$$\sigma_k = \frac{f_t \left(\frac{2G_F}{f_t} - w_1\right)}{w_c - w_1} \tag{A.2}$$

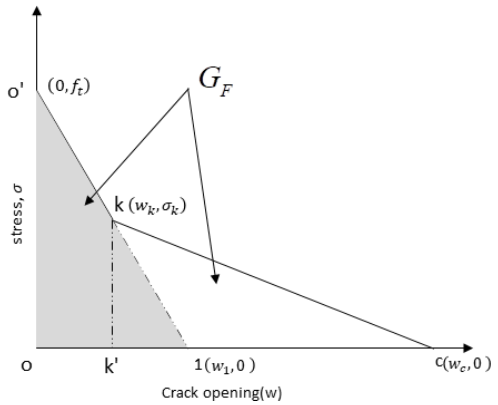

Fig. A.1 The typical bilinear curve of concrete

According to Fig. A.1, given the similarity of the triangles KK'1and O'O1, relation (A.3) is written as

$$\frac{\sigma_k}{f_t} = 1 - \frac{w_k}{w_1} \tag{A.3}$$

By substituting Eq. (A.2) for σ_k ,w_k is written as

$$w_k = w_1 \frac{w_c - 2(\frac{G_F}{f_t})}{w_c - w_1} \tag{A.4}$$

B. Finding a quadratic equation in terms of w_c

The abscissa $\overline{w}$ of the center of gravity of the area defined by the curve and the axes is

calculated by

$$\overline{w} = \frac{\sum A_i \overline{w_i}}{\sum A_i} \tag{A.5}$$

According to Fig. A.1, the softening curve could be considered as two separated triangles o' o1 and k1c. By using Eq. (A.5) for finding the abscissa of the center of gravity, Eq. (A.6) is generated.

$$\overline{w} = \frac{\frac{f_t w_1^2}{6} + \left(\frac{(w_1 - w_k) + (w_c - w_k)}{3} + w_k\right)(G_F - \frac{f_t w_t^2}{6})}{G_F} \tag{A.6}$$

Eq. (A.6) is rearranged and rewritten as Eq. (A.7).

$$\overline{w} G_F = \frac{f_t w_1^2}{6} + \left(\frac{w_1 + w_c + w_k}{3}\right)(G_F - \frac{f_t w_t^2}{6}) \tag{A.7}$$

By substituting Eq. (A.4) for w_k , Eq. (A.7) is written as Eq. (A.8).

$$\overline{w} G_F = \frac{f_t w_1^2}{6} + \left(\frac{1}{3}\right)\left(w_1 + w_c + w_1 \frac{w_c - 2(\frac{G_F}{f_t'})}{w_c - w_1}\right)(G_F - \frac{f_t w_t^2}{6}) \tag{A.8}$$

Rearranging the Eq. (A.8) reproduce quadratic equation in terms of w_c. Solving this equation leads to find w_c after finding $\overline{w}$ in each step, as mentioned before.

$$w_c^2 - w_c \frac{6\overline{w}\left(\frac{G_F}{f_t'}\right) - 2w_1\left(\frac{G_F}{f_t'}\right)}{2\left(\frac{G_F}{f_t'}\right) - w_1} + \frac{6\overline{w} w_1\left(\frac{G_F}{f_t'}\right) - 4w_1\left(\frac{G_F}{f_t'}\right)^2}{2\left(\frac{G_F}{f_t'}\right) - w_1} = 0 \tag{A.9}$$